Available online at www.sciencedirect.com

ScienceDirect

IFAC PapersOnline CONFERENCE PAPER ARCHIVE

IFAC PapersOnLine 59-8 (2025) 84–89

PDE Modeling of the Cooling Fluid Temperature in Battery Pack

Patryck Ferreira * **Shu-Xia Tang** *

* *Department of Mechanical Engineering, Texas Tech University (e-mail: patferre@ttu.edu, shuxia.tang@ttu.edu)*

Abstract: This paper presents a comprehensive analysis of heat transfer in cooling systems for battery packs in electric vehicles (EVs). A cylindrical coordinate framework is employed to model the heat transfer equation, incorporating diffusion, convection, and heat sources due to electrochemical reactions in the cell. Boundary conditions are derived to account for radial symmetry and cascaded axial heat exchange across modules. The proposed model introduces a coupled nonlinear framework that dynamically interrelates fluid temperature, heat generation, and module temperature, effectively capturing transient and nonlinear thermal interactions.

Keywords: Cooling Fluid Temperature, Electric Vehicle Cooling, Laminar Flow, Battery Pack, Lithium ion Batteries

1. INTRODUCTION

Battery packs are fundamental components in numerous applications, notably in electric vehicles (EVs), renewable energy storage systems, and portable electronic devices. According to Ferreira and Tang [2024a], a battery pack consists of multiple interconnected battery cells arranged in series or parallel configurations, along with supporting components such as a battery management system (BMS), cooling mechanisms, and a protective casing. As described in Safavi et al. [2024], the BMS plays a crucial role in monitoring the condition of the batteries through the state-of-health (SoH), defined as the ratio of the current capacity to the initial capacity. Additionally, Jafari and Byun [2024] states that the BMS regulates battery temperature to prevent thermal runaway or explosion. According to International Energy Agency [2020], lithium-ion battery packs in electric vehicles (EVs) serve as the primary energy storage system, enabling the transition away from fossil fuels and supporting global sustainability goals. The performance, safety, and lifespan of these battery packs are highly sensitive to temperature variations, highlighting the importance of effective thermal management systems (TMS), as emphasized in Pesaran [2013].

According to Bandhauer et al. [2011] the thermal behavior of lithium-ion batteries is influenced by exothermic reactions during operation . As described in Feng et al. [2018], elevated temperatures can accelerate degradation, reduce capacity, and, in severe cases, trigger thermal runaway, posing significant safety risks . Conversely, low temperatures can lead to decreased efficiency and power output. To manage these thermal challenges, heat exchangers are integral components of EV battery packs, enabling efficient regulation of battery temperatures. These systems are broadly classified based on their cooling methods and structural designs. As noted in Huo et al. [2015], air cooling is the simplest method and relies on ambient or forced airflow to dissipate heat. According to Kim et al. [2007], liquid cooling favored for its superior heat transfer efficiency uses coolant flowing through plates, tubes, or channels in direct contact with the battery cells. Additionally, Saw et al. [2016] states that cooling plates, whether flat or contoured, are widely implemented due to their compact design and effective thermal performance. As described in Møller et al. [2017], immersion cooling, in which battery cells are submerged in a dielectric fluid, offers exceptional temperature uniformity by enabling direct contact with the cell surfaces. Finally, Kizilel et al. [2009] presents phase change materials as an alternative solution, absorbing heat through phase transitions within specific temperature ranges.

This study aims to enhance the design and modeling of cooling systems in EV battery packs that employ pipes and a water–glycol mixture as the cooling fluid. The battery pack structure is inspired by the Tesla Model S design, as described in Bhowmick [2021], and further refined using insights from recent advancements presented in Ferreira and Tang [2024a]. The key contributions of this work are summarized as follows:

- Introduction of a coupled, nonlinear framework that dynamically interrelates fluid temperature, heat generation, and module temperature, effectively addressing transient and nonlinear thermal interactions.
- Explicit consideration of cascaded thermal interactions between battery modules, reflecting realistic designs such as the Tesla Model S.
- Integration of detailed velocity field assumptions into the heat transfer model, improving the physical accuracy of temperature predictions.

2. TEMPERATURE DISTRIBUTION IN COOLING PIPES FOR ELECTRIC VEHICLES.

Temperature in the cooling system of EVs is critical for ensuring the safety and reliability of battery packs. Figure 1 **(A)** provides a schematic representation of the entire bat-

10.1016/j.ifacol.2025.08.071

tery pack, showing the arrangement of battery modules, the pack housing, and the flow of cooling fluid through the heat exchange system. Figure 1 **(B)** focuses on a zoomed-in view of the thermal interaction between the cooling fluid in the heat exchanger pipe and the battery modules. The cooling fluid temperature, denoted as $T_{\text{fluid},i}$, flows through pipes from z_0 to z_5, thermally interacting with the modules, which contribute heat represented by $T_{\text{m},i}$. Here, i indexes the fluid regions adjacent to each battery module boundary, where thermal interaction takes place, with $i = \overline{1,8}$. The system demonstrates sequential thermal interactions, where the fluid temperature evolves as it passes through each module, highlighting the cascaded structure of the thermal exchange process.

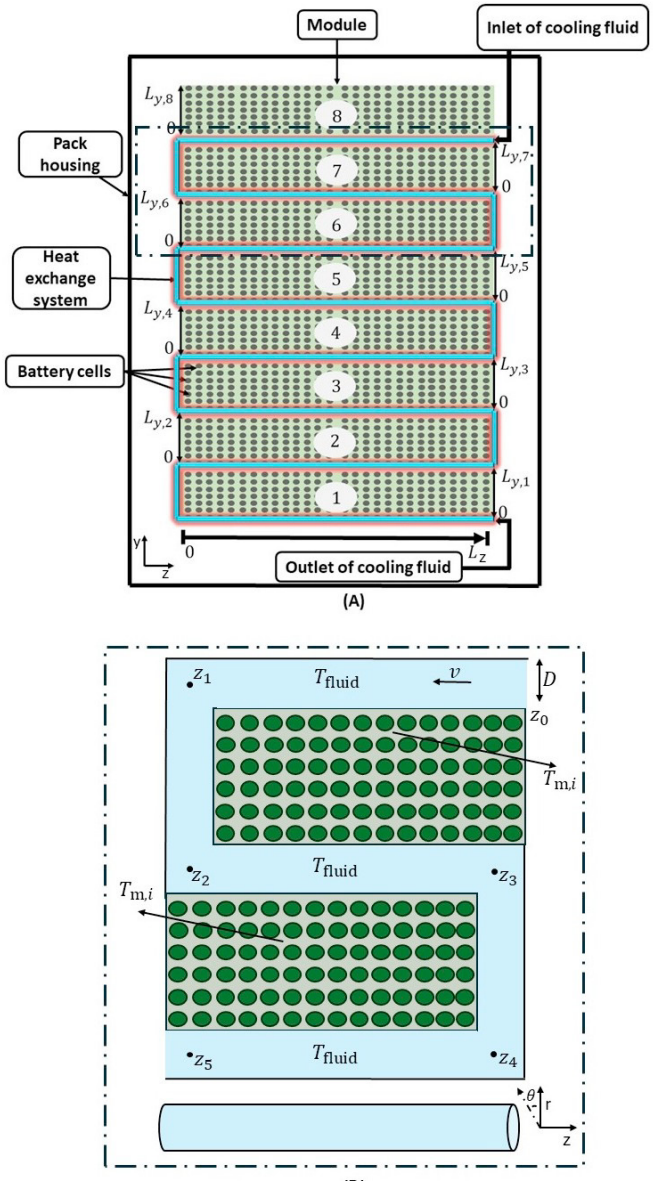

Fig. 1. **(A)** Schematic representation of the battery pack, showing the arrangement of modules and the cooling system. **(B)** Zoomed-in view of the dashed box, illustrating the system in cylindrical coordinates.

Assumption 1. *The flow is symmetric about the azimuthal coordinate θ, reducing the problem to two spatial dimensions, r and z.*

To accurately determine this temperature, this article introduces the transient convection–diffusion equation in cylindrical coordinates:

$$\frac{\partial T_{\text{fluid},i}(t,r,z)}{\partial t} = \alpha\left[\frac{1}{r}\frac{\partial}{\partial r}\left(r\frac{\partial T_{\text{fluid},i}(t,r,z)}{\partial r}\right) + \frac{\partial^2 T_{\text{fluid},i}(t,r,z)}{\partial z^2}\right] - \left(v_r(t,r,z)\frac{\partial T_{\text{fluid},i}(t,r,z)}{\partial r} + v_z(t,r,z)\frac{\partial T_{\text{fluid},i}(t,r,z)}{\partial z}\right) + Q_i(t,r,z), \quad (1)$$

where $T_{\text{fluid},i}(t,r,z)$ represents the fluid temperature, α is the thermal diffusivity, $v_r(t,r,z)$ and $v_z(t,r,z)$ are the components of velocity in the radial and axial directions, respectively, and $Q_i(t,r,z)$ is the heat source term. Note that (1) should hold piecewise.

2.1 Velocities Profiles $v_r(t,r,z)$ and $v_z(t,r,z)$

The primary difficulty in Equation (1) arises from the velocity terms. To aid in their interpretation, the following assumptions are introduced.

Assumption 2. *The velocity field is assumed to be incompressible, laminar, and steady (no acceleration), meaning the fluid density remains constant, the flow is smooth and orderly, and the velocity components do not change with time ($\frac{\partial v_r}{\partial t} = 0$ and $\frac{\partial v_z}{\partial t} = 0$).*

Assumption 3. *Due to the symmetry of the flow and the absence of significant radial variations along the axial direction (z), the radial velocity $v_r(r,z)$ is simplified to depend only on the radial coordinate r, resulting in $v_r = v_r(r)$. In contrast, the axial velocity v_z depends on both r and z, $v_z = v_z(r,z)$, due to axial pressure gradients and heat transfer effects that vary along the pipe length.*

Assumption 4. *The pressure gradient $\frac{\mathrm{d}P(z)}{\mathrm{d}z}$ is averaged over the entire pipe length L, accounting for axial variations in the velocity profile $v_z(r,z)$. Based on this, the average velocity v_{avg} is assumed to be constant.*

Under these conditions, the incompressible continuity equation, $\frac{1}{r}\frac{\partial(rv_r)}{\partial r} + \frac{\partial v_z}{\partial z} = 0$, must hold.

Radial Velocity $v_r(r)$: Figure 2 illustrates the free-body diagram laminar flow in a horizontal pipe and the forces acting on a ring-shaped differential fluid element as discussed in [Yunus, 2010, Chapter 8, Section 8.4]. The parabolic profile highlights that the velocity is maximum at the centerline ($v_{\max}$) and decreases to zero at the wall due to the no-slip condition. The balance of axial pressure forces (P_z and $P_z + \Delta P$) and radial shear stresses (τ_r and $\tau_r + \Delta\tau_r$) ensures steady flow.

The maximum velocity in this context is assumed to be the highest fluid velocity achievable by the pump. As presented in [Yunus, 2010, Chapter 8, Section 8.4], the average velocity

$$v_{\text{avg}} = \frac{v_{\max}}{2}. \quad (2)$$

To determine the velocity in the radial direction, the force balance for a fluid element along the axial direction is considered. Referring to Figure 2, this leads to:

$$(2\pi r\,\Delta r\,P(z)) - (2\pi r\,\Delta r\,P(z+\Delta z) + (2\pi r\,\Delta z\,\tau_r(r)) - (2\pi r\,\Delta z\,\tau_r(r+\Delta r) = 0. \quad (3)$$

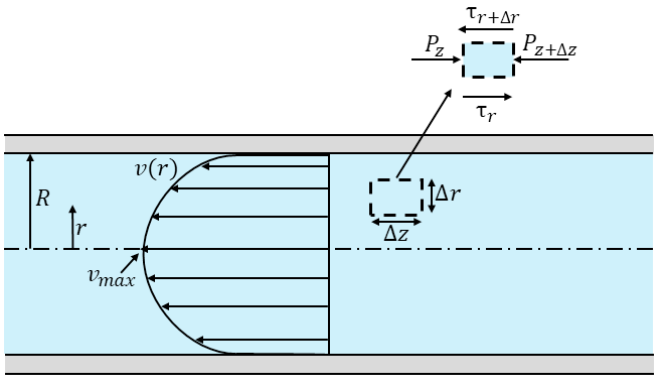

Fig. 2. Schematic representation of the velocity profile and forces acting on a fluid element in a horizontal pipe.

This indicates that, for steady, fully developed laminar flow in a horizontal pipe, viscous forces exactly balance the pressure forces. Dividing (3) by $2\pi r\,\Delta r\,\Delta z$ and simplifying yields:

$$\frac{P(z+\Delta z)-P(z)}{\Delta z}+\frac{(r\tau_r(r))_{r+\Delta r}-(r\tau_r(r))}{\Delta r}=0. \quad (4)$$

Taking the limit as $\Delta r\to 0, \Delta z\to 0$:

$$r\frac{\mathrm{d}P(z)}{\mathrm{d}z}+\frac{\mathrm{d}(r\tau_r(r))}{\mathrm{d}r}=0. \quad (5)$$

Substituting $\tau_r(r)=-\mu\frac{\mathrm{d}v_r(r)}{dr}$ and assuming constant viscosity μ, the governing equation becomes:

$$\frac{\mu}{r}\frac{\mathrm{d}}{\mathrm{d}r}\left(r\frac{\mathrm{d}v_r(r)}{\mathrm{d}r}\right)=\frac{\mathrm{d}P(z)}{\mathrm{d}z}. \quad (6)$$

Assuming a constant pressure gradient $\frac{\mathrm{d}P(z)}{\mathrm{d}z}$, Equation (6) is integrated twice with respect to r to yield the general velocity profile:

$$v_r(r)=\frac{r^2}{4\mu}\frac{\mathrm{d}P(z)}{dz}+C_1\ln r+C_2, \quad (7)$$

where the constants C_1, C_2 are to be determined.

The following boundary conditions hold:

$$v_r(R)=0 \qquad \text{(no-slip condition at the wall)}, \quad (8)$$

$$\left.\frac{\mathrm{d}v_r(r)}{\mathrm{d}r}\right|_{r=0}=0 \qquad \text{(symmetry at the centerline)}. \quad (9)$$

Based on (9), the constant C_1 is set to zero. Then, C_2 is determined by applying (8), resulting in $C_2=-\frac{R^2}{4\mu}\frac{\mathrm{d}P(z)}{\mathrm{d}z}$. Substituting these constants into (7) yields

$$v_r(r)=-\frac{R^2}{4\mu}\frac{\mathrm{d}P(z)}{\mathrm{d}z}\left(1-\frac{r^2}{R^2}\right). \quad (10)$$

The average velocity v_{avg} is determined by integrating the velocity profile over the pipe's cross-sectional area:

$$v_{\text{avg}}=\frac{2}{R^2}\int_0^R v_r(r)r\,\mathrm{d}r=\frac{-R^2}{8\mu}\frac{\mathrm{d}P(z)}{\mathrm{d}z}. \quad (11)$$

The velocity profile can be rewritten in terms of v_{avg}:

$$v_r(r)=2v_{\text{avg}}\left(1-\frac{r^2}{R^2}\right). \quad (12)$$

Axial Velocity $v_z(r,z)$: According to [Yunus, 2010, Chapter 9, Section 9.1], the incompressible continuity equation in cylindrical coordinates is:

$$\frac{1}{r}\frac{\partial(rv_r)}{\partial r}+\frac{1}{r}\frac{\partial v_\theta}{\partial\theta}+\frac{\partial v_z}{\partial z}=0. \quad (13)$$

Under Assumption 1, which implies axisymmetry ($\frac{\partial v_\theta}{\partial\theta}=0$) and incompressibility, the continuity equation simplifies to:

$$\frac{1}{r}\frac{\partial(rv_r(r))}{\partial r}+\frac{\partial v_z(r,z)}{\partial z}=0. \quad (14)$$

Multiplying (12) by r:

$$rv_r(r)=2v_{\text{avg}}\left(r-\frac{r^3}{R^2}\right), \quad (15)$$

its derivative with respect to r is:

$$\frac{\partial(rv_r(r))}{\partial r}=2v_{\text{avg}}\left(1-\frac{3r^2}{R^2}\right). \quad (16)$$

Substituting into the continuity equation gives:

$$\frac{\partial v_z(r,z)}{\partial z}=-\frac{2v_{\text{avg}}}{r}\left(1-\frac{3r^2}{R^2}\right). \quad (17)$$

The boundary conditions are:

$$\left.\frac{\partial v_z(r,z)}{\partial r}\right|_{r=0}=0 \qquad \text{(symmetry at the centerline)}, \quad (18)$$

$$v_z(R,z)=0 \qquad \text{(no-slip condition at the wall)}, \quad (19)$$

integrating with respect to z, we obtain:

$$v_z(r,z)=v_z(r,0)-z\cdot\frac{2v_{\text{avg}}}{r}\left(1-\frac{3r^2}{R^2}\right), \quad (20)$$

where $v_z(r,0)$ represents the inlet velocity profile at the entry point of the system, driven by the pump. For $r>0$, the velocity fields satisfy the incompressible axisymmetric continuity equation, ensuring conservation of mass throughout the flow domain. Although the expression is singular at the centerline ($r=0$), this can be addressed by enforcing symmetry and regularity conditions, ensuring smooth and physically meaningful solutions both analytically and numerically.

Verification of Mass Conservation in Axisymmetric Flow: From Equation (16), divide by r as required in the continuity equation:

$$\frac{1}{r}\frac{\partial(rv_r(r))}{\partial r}=\frac{2v_{\text{avg}}}{r}\left(1-\frac{3r^2}{R^2}\right). \quad (21)$$

The derivative with respect to z is given by Equation (17):

$$\frac{\partial v_z(r,z)}{\partial z}=-\frac{2v_{\text{avg}}}{r}\left(1-\frac{3r^2}{R^2}\right). \quad (22)$$

Thus, the derived velocity fields $v_r(r)$ and $v_z(r,z)$ satisfy the incompressible axisymmetric continuity equation:

$$\frac{1}{r}\frac{\partial(rv_r)}{\partial r}+\frac{\partial v_z}{\partial z}=0, \quad (23)$$

ensuring that the derived velocity fields are consistent with the fundamental principle of mass conservation throughout the flow field.

2.2 Heat Source Term $Q_i(t, r, z)$

The heat that must be removed by the cooling pipe to maintain the battery pack within safe operating conditions is governed by Newton's Law of Cooling, expressed as:

$$Q_i(t,r,z) = \frac{h_{\text{conv,ex}} A_{\text{conv,ex}} \left(T_{\text{m},i}(t,z,y) - T_{\text{fluid},i}(t,r,z)\right)}{v_{\text{fluid}}\, \rho_{\text{fluid}}\, c_{p,\text{fluid}}}, \tag{24}$$

where $h_{\text{conv,ex}}$ is the convective heat transfer coefficient of the cooling fluid, $A_{\text{conv,ex}}$ is the heat transfer surface area of the pipe in contact with the fluid, $T_{\text{m},i}(t,z,y)$ is the temperature of the battery module, v_{fluid} is the volume of fluid, ρ_{fluid} is the fluid density, $c_{p,\text{fluid}}$ is the heat capacity of the fluid, and $T_{\text{fluid},i}(t,r,z)$ is the temperature of the cooling fluid, which is the primary variable being solved. $T_{\text{m}_i}(t,z,y)$ was first developed in Ferreira and Tang [2024a], there $T_{\text{fluid},i}(t,r,z)$ was constant, here we are going to couple everything. The module $T_{\text{m},i}(t,y,z)$ is given by:

$$\frac{\partial T_{\text{m},i}(t,z,y)}{\partial t} = \alpha \left(\frac{\partial^2 T_{\text{m},i}(t,z,y)}{\partial z^2} + \frac{\partial^2 T_{\text{m},i}(t,z,y)}{\partial y^2} \right) + Q_{\text{module}}(t), \tag{25}$$

where α denotes the thermal diffusivity, and $Q_{\text{module}}(t)$ is the module heat generation given by:

$$Q_{\text{module}}(t) = \frac{n Q_{\text{cell}}(t)}{v_{\text{module}} \rho_{\text{module}} c_{\text{p,module}}}, \tag{26}$$

where n is the number of cell in the module, $Q_{\text{cell}}(t)$ is the heat generated in each cell, v_{module} is the volume of the module, and ρ_{module}, $c_{\text{p,module}}$ are the density and heat capacity of the module's material.

The generated heat $Q_{\text{cell}}(t)$ is divided into three components, as discussed in Ferreira and Tang [2024a]: one for electrochemical reactions, $S_{\text{cell}}(t)$; another for the conduction interaction between the components, $q^*_{\text{cond,cell}}$; and the last one pertaining to the convective heat transfer of the electrolyte, represented as $q^*_{\text{conv,cell}}$,it is described as:

$$Q_{\text{cell}}(t) = S_{\text{cell}}(t) + q^*_{\text{cond,cell}} + q^*_{\text{conv,cell}}. \tag{27}$$

Electrochemical Heat Generation: The electrochemical heat generation term, $S_{\text{cell}}(t)$, based on the Single Particle Model (SPM), is discussed in Ferreira and Tang [2024b] and is represented as:

$$S_{\text{cell}}(t) = V(t)|I(t)|, \tag{28}$$

where $V(t)$ denotes the voltage determined by the electrochemical model, while $I(t)$ represents the current applied to the battery. Taking the absolute value $|I(t)|$ guarantees that the thermal power is always positive, as heat generation is intrinsically positive, irrespective of whether the current flows during charging or discharging.

Figure 3 illustrates the Single Particle Model (SPM), a reduced-order electrochemical model that represents each electrode as a single spherical particle to efficiently simulate lithium diffusion and voltage, while neglecting spatial variations across the electrode thickness. The terminal voltage is given by the difference between the solid-phase potentials of the electrodes, where concentration of lithium ions in the electrodes follows Fick's law of diffusion, expressed as:

$$\begin{aligned}
\frac{\partial c_s^{\pm}}{\partial t}(t,r_s) &= \frac{1}{r_s^2}\frac{\partial}{\partial r_s}\left[D_s^{\pm}(T(t)) r_s^2 \frac{\partial c_s^{\pm}}{\partial r_s}(t,r_s)\right], \\
&\quad t>0, \quad r_s \in (0, R_s^{\pm}), \\
\frac{\partial c_s^{\pm}}{\partial r_s}(t,0) &= 0, \quad t>0, \\
\frac{\partial c_s^{\pm}}{\partial r_s}(t,R_s^{\pm}) &= -\frac{1}{D_s^{\pm}(T(t))} j^{\pm}(t), \quad t>0, \\
c_s^{\pm}(0,r_s) &= c_{s,0}^{\pm}(r_s), \quad r_s \in [0, R_s^{\pm}],
\end{aligned}$$

where the spatial variable is r_s, the solid phase $c_s^{\pm} \in \mathbb{R}$, $D_s^{\pm}$ is the diffusion coefficient of the solid phase, and $j^{\pm}$ is the molar flux given by:

$$j^+(t) = -\frac{I(t)}{a_s^+ F L^+}, \quad j^-(t) = \frac{I(t)}{a_s^- F L^-},$$

where $a_s^{\pm}$ stands for the interfacial surface area, F denotes the Faraday constant, and $L^{\pm}$ corresponds to the length of the positive or negative electrode.

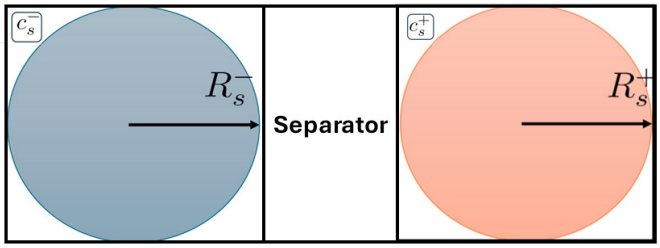

Fig. 3. Single Particle Model (SPM).

Heat Generated Due to Conduction: The heat generated due to conduction, denoted as $q^*_{\text{cond,cell}}$, is defined as:

$$q^*_{\text{cond,cell}} = \frac{T^*_{\text{core}} - T^*_{\text{case}}}{R_{\text{cell}}}, \tag{29}$$

where T_{core} represents the core temperature, T_{case} represents the temperature of the case, and R_{cell} denotes the total thermal resistance of the material in the spiral:

$$R_{\text{cell}} = \frac{\ln(r_2/r_1)}{2\pi k_s L_{\text{cell}}}, \tag{30}$$

where r_1 represents the internal radius of the cell, r_2 represents the external radius of the cell, L_{cell} represents the length of the spiral, and k_s represents the thermal conductivity of the material in the spiral, as described in [Bergman et al., 2011, Chapter 3, Section 3.3.1].

Heat Generated Due to Convection: The convective heat transfer between the electrolyte and the spiral follows Newton's law of cooling, expressed as:

$$q^*_{\text{conv,cell}} = h_{\text{cell}} A_{\text{cell}} (T^*_{\text{e}} - T^*_{\text{spiral}}), \tag{31}$$

where h_{cell} represents the convective heat transfer coefficient of the electrolyte, A_{cell} is the area covered by the electrolyte, T^*_{e} is the electrolyte temperature, and T^*_{spiral} denotes the temperature of the spiral inside the battery.

Boundary Conditions for Module Temperature $T_{m,i}$: For odd-numbered modules, this interaction takes place over the domains $(0,\infty) \times [0, L_z] \times [0, L_{y,i}]$. The boundary conditions for odd-numbered modules $i = 7, 5, 3, 1$, where

contact with ambient air occurs solely on the right side, the boundary conditions are as follows:

$$
\begin{aligned}
&T_{\mathrm{m},i}(t,z,L_{y,i}) = T_{\mathrm{fluid}}(t,r,z) + \frac{q_{\mathrm{conv,ex},i}}{2k}(l_z^2 - z^2) \\
&+ \left(\frac{T_i^*}{(l_z + L_z)} - \frac{T_{\mathrm{fluid}}(t,r,z)}{(l_z + L_z)} - \frac{q(l_z^2 - L_z^2)}{2k(l_z + L_z)} \right)(l_z + z), \\
&\quad \forall (t,z) \in (0,\infty) \times [0, L_z], \\
&T_{\mathrm{m},i}(t,z,0) = T_{\mathrm{fluid}}(t,r,z) + \frac{q_{\mathrm{conv,ex},i}}{2k}(l_z^2 - z^2) \\
&+ \left(\frac{T_{i-1}^*}{(l_z + L_z)} - \frac{T_{\mathrm{fluid}}(t,r,z)}{(l_z + L_z)} - \frac{q(l_z^2 - L_z^2)}{2k(l_z + L_z)} \right)(l_z + z), \\
&\quad \forall (t,z) \in (0,\infty) \times [0, L_z], \\
&T_{\mathrm{m},i}(t,0,y) = T_{\mathrm{fluid}}(t,r,z) + \frac{q_{\mathrm{conv,ex},i}}{2k}(l_y^2 - y^2) \\
&+ \left(\frac{T_i^*}{(l_y + L_{y,i})} - \frac{T_{\mathrm{fluid}}(t,r,z)}{(l_y + L_{y,i})} - \frac{q(l_y^2 - L_{y,i}^2)}{2k(l_y + L_{y,i})} \right)(l_y + y), \\
&\quad \forall (t,y) \in (0,\infty) \times [0, L_{y,i}], \\
&T_{\mathrm{m},i}(t,L_z,y) = T_{\mathrm{air}}, \quad \forall (t,y) \in (0,\infty) \times [0, L_{y,i}].
\end{aligned} \tag{32}
$$

For even-numbered modules, this interaction takes place over the domains $(0,\infty) \times [0, L_z] \times [0, L_{y,i}]$. The boundary conditions for even-numbered modules $i = 6, 4, 2$, where contact with ambient air is present only on the left side, the boundary conditions are as follows:

$$
\begin{aligned}
&T_{\mathrm{m},i}(t,z,L_{y,i}) = T_{\mathrm{fluid}}(t,r,z) + \frac{q_{\mathrm{conv,ex},i}}{2k}(l_z^2 - z^2) \\
&+ \left(\frac{T_i^*}{(l_z + L_z)} - \frac{T_{\mathrm{fluid}}(t,r,z)}{(l_z + L_z)} - \frac{q(l_z^2 - L_z^2)}{2k(l_z + L_z)} \right)(l_z + z), \\
&\quad \forall (t,z) \in (0,\infty) \times [0, L_z], \\
&T_{\mathrm{m},i}(t,z,0) = T_{\mathrm{fluid}}(t,r,z) + \frac{q_{\mathrm{conv,ex},i}}{2k}(l_z^2 - z^2) \\
&+ \left(\frac{T_{i-1}^*}{(l_x + L_z)} - \frac{T_{\mathrm{fluid}}(t,r,z)}{(l_z + L_z)} - \frac{q(l_z^2 - L_z^2)}{2k(l_z + L_z)} \right)(l_z + z), \\
&\quad \forall (t,z) \in (0,\infty) \times [0, L_z], \\
&T_{\mathrm{m},i}(t,0,y) = T_{\mathrm{air}}, \quad \forall (t,y) \in (0,\infty) \times [0, L_{y,i}], \\
&T_{\mathrm{m},i}(t,L_z,y) = T_{\mathrm{fluid}}(t,r,z) + \frac{q_{\mathrm{conv,ex},i}}{2k}(l_z^2 - y^2) \\
&+ \left(\frac{T_i^*}{(l_y + L_{y,i})} - \frac{T_{\mathrm{fluid}}(t,r,z)}{(l_z + L_{y,i})} - \frac{q(l_y^2 - L_{y,i}^2)}{2k(l_y + L_{y,i})} \right)(l_y + z), \\
&\quad \forall (t,y) \in (0,\infty) \times [0, L_{y,i}].
\end{aligned} \tag{33}
$$

Here,

$$
q_{\mathrm{conv,ex},i} = h_{\mathrm{conv,ex}} A_{\mathrm{conv,ex}} (T_i^* - T_{\mathrm{fluid}}), \tag{34}
$$

where $h_{\mathrm{conv,ex}}$ represents the local convection heat transfer coefficient, $A_{\mathrm{conv,ex}}$ denotes the internal area of the cooling system, T_i^* signifies the temperature of each module in contact with the heat exchange system wall:

$$
T_i^* = \frac{A_{\mathrm{conv,ex}} h_{\mathrm{conv,ex}} T_{\mathrm{fluid}}^* R_i - T_{i-1}^*}{A_{\mathrm{conv,ex}} h_{\mathrm{conv,ex}} R_i - 1}, \tag{35}
$$

where R_i is the module's thermal resitance.

2.3 Boundary Conditions for the Heat Equation

Figure 1 **(B)** illustrates the cooling system for two modules, serving as an example to define the boundary conditions for this system.

Assumption 5. *In curved sections of the pipe, the flow remains laminar with no vortices, as the Reynolds number indicates stable and smooth flow. This ensures that the heat transfer analysis remains valid and unaffected by turbulence or additional mixing effects.*

In the radial direction (r), the boundary conditions are:

$$
\left. \frac{\partial T_{\mathrm{fluid},i}(t,r,z)}{\partial r} \right|_{r=0} = 0, \tag{36}
$$

indicating no radial heat flux at the pipe centerline due to symmetry. At the pipe wall ($r = R$):

$$
T_{\mathrm{fluid},i}(t,r,z)|_{r=R} = T_{\mathrm{case}}(t,r,z), \tag{37}
$$

where T_{case} is the external surface temperature of the pipe in contact with the module. The dependence on y is not included in T_{case} since it is assumed to be uniform along the module height at the interface.

In the axial direction (z), the boundary conditions follow a cascaded structure. At the inlet of the first section ($z = z_0$), the initial fluid temperature is specified as:

$$
T_{\mathrm{fluid},i}(t,r,z)|_{z=z_0} = T_0(t,r,z), \tag{38}
$$

where T_0 is the known fluid temperature entering the cooling pipe.

At the end of the first module section ($z = z_1$), the axial heat flux is governed by the temperature difference between the module and the fluid at the pipe surface:

$$
\left. \frac{\partial T_{\mathrm{fluid},i}(t,r,z)}{\partial z} \right|_{z=z_1} = hA \left(T_{\mathrm{m},i}(t,z,y) - T_{\mathrm{case}}(t,r,z) \right), \tag{39}
$$

where $T_{\mathrm{m},i}(t,z,y)$ is the temperature of the i-th battery module interacting with the fluid at axial position z and vertical position y.

For subsequent sections ($z = z_2, z_3, \ldots, z_n$), the boundary condition is cascaded to reflect sequential module interactions:

$$
\left. \frac{\partial T_{\mathrm{fluid},i}(t,r,z)}{\partial z} \right|_{z=z_i} = hA \left(T_{\mathrm{m},i}(t,z,y) - T_{\mathrm{fluid},i-1}(t,r,z) \right), \tag{40}
$$

where $T_{\mathrm{fluid},i-1}(t,r,z)$ denotes the fluid temperature computed from the previous module section at $z = z_{i-1}$.

These boundary conditions capture both radial and axial heat transfer, accommodating the cascaded structure of the cooling system with sequential module interactions.

2.4 The Full Transient Convection–Diffusion Equation

Equations (24) and (25) establish a tightly coupled relationship among the fluid temperature $T_{\mathrm{fluid},i}(t,r,z)$, the module temperature $T_{\mathrm{m},i}(t,z,y)$, and the heat flux $Q_i(t,r,z)$. The heat flux $Q_i(t,r,z)$ depends on $T_{\mathrm{fluid},i}(t,r,z)$, which varies spatially and temporally, while $T_{\mathrm{fluid},i}(t,r,z)$ is governed by the heat equation with $Q_i(t,r,z)$ as a source term. This nonlinear coupling is further complicated by the dependence of $T_{\mathrm{m},i}(t,z,y)$ on $T_{\mathrm{fluid},i}(t,r,z)$, creating an intricate feedback mechanism that makes solving the system challenging. Substituting $Q_i(t,r,z)$ into Equation (1), the heat equation becomes:

$$\frac{\partial T_{\text{fluid},i}(t,r,z)}{\partial t} = \alpha \left[\frac{1}{r}\frac{\partial}{\partial r}\left(r\frac{\partial T_{\text{fluid},i}(t,r,z)}{\partial r}\right) + \frac{\partial^2 T_{\text{fluid},i}(t,r,z)}{\partial z^2}\right] - \left(v_r(r)\frac{\partial T_{\text{fluid},i}(t,r,z)}{\partial r} + v_z(r,z)\frac{\partial T_{\text{fluid},i}(t,r,z)}{\partial z}\right) + \frac{h_{\text{conv,ex}}A_{\text{conv,ex}}\left(T_{\text{m},i}(t,z,y) - T_{\text{fluid},i}(t,r,z)\right)}{v_{\text{fluid}}\,\rho_{\text{fluid}}\,c_{p,\text{fluid}}}. \quad (41)$$

The term $-h_{\text{conv,ex}}A_{\text{conv,ex}}T_{\text{fluid},i}(t,r,z)$ represents a heat sink, capturing energy removed from the fluid, while $h_{\text{conv,ex}}A_{\text{conv,ex}}T_{\text{m},i}(t,z,y)$ acts as a heat source from the module to the fluid. The appearance of $T_{\text{fluid},i}(t,r,z)$ in both the governing equation and heat transfer terms highlights the strong coupling between fluid and module temperatures. This nonlinear interaction, driven by spatially and temporally varying $T_{\text{fluid},i}$ and $T_{\text{m},i}$, complicates the model. Since $Q_i(t,r,z)$ depends on $T_{\text{fluid},i}(t,r,z)$, and $T_{\text{m},i}(t,z,y)$ is influenced by $T_{\text{fluid},i}$ through boundary conditions, the system is highly coupled and nonlinear. The equations are discretized using finite element methods and solved iteratively via a Newton-based solver to ensure numerical stability and accuracy. Boundary conditions enforce radial symmetry, continuity, and ambient interactions. This modeling framework enables realistic transient thermal simulations and provides a foundation for optimizing battery thermal management systems. Model validation will be addressed in future work.

Table 1 presents the logical structure for calculating the temperature of the cooling fluid in the battery pack.

Table 1. Cooling Fluid Temperature in a Battery Pack.

Velocity profiles: (12), (20)
Heat generation in the cooling fluid: (24)
Module temperature, boundary conditions, and heat generation: (25),(26), (32), and (33)
Fluid boundary conditions: (36), (37), (38), (39)
Finally, solve the fluid PDE: (1)

3. CONCLUSION AND FUTURE WORK

This study introduces a mathematical model for the thermal behavior of EV battery pack cooling systems, capturing the nonlinear coupling between fluid temperature, module temperature, and heat generation. Although simulation results are not included due to space constraints, the model provides a foundation for optimizing thermal management systems.

Future work will involve numerical validation using finite difference methods with implicit time integration and iterative solvers, such as Newton's method. The model will be extended to include pressure variation, and its predictions will be validated against experimental data, with a focus on temperature uniformity, velocity distribution, and pressure drop. Additionally, the model will support parametric studies to optimize fluid properties and system geometry.

REFERENCES

Bandhauer, T.M., Garimella, S., and Fuller, T.F. (2011). A critical review of thermal issues in lithium-ion batteries. *Journal of the electrochemical society*, 158(3), R1.

Bergman, T., Lavine, A., and DeWitt, D. (2011). *Introduction to Heat Transfer*. Wiley, Hoboken, NJ, 6th edition.

Bhowmick, S. (2021). Tesla model s battery system: An engineer's perspective. *Circuit Digest*. URL `https://circuitdigest.com/article/tesla-model-s-battery-system-an-engineers-perspective`. Accessed: 2025-01-15.

Feng, X., Ouyang, M., Liu, X., Lu, L., Xia, Y., and He, X. (2018). Thermal runaway mechanism of lithium ion battery for electric vehicles: A review. *Energy storage materials*, 10, 246–267.

Ferreira, P. and Tang, S.X. (2024a). Advancement in lithium-ion battery pack thermal modeling based on electrochemical principles. In *Heat Transfer Summer Conference*, volume 87905. American Society of Mechanical Engineers.

Ferreira, P. and Tang, S.X. (2024b). Sensors placement analysis and temperature estimation in lithium-ion batteries with a cascaded electrochemical-thermal model. In *2024 European Control Conference (ECC)*, 200–205.

Huo, Y., Rao, Z., Liu, X., and Zhao, J. (2015). Investigation of power battery thermal management by using mini-channel cold plate. *Energy Conversion and Management*, 89, 387–395.

International Energy Agency (2020). Global EV Outlook 2020. `https://www.iea.org/reports/global-ev-outlook-2020`. Accessed: 2024-12-06.

Jafari, S. and Byun, Y.C. (2024). Efficient state of charge estimation in electric vehicles batteries based on the extra tree regressor: A data-driven approach. *Heliyon*, 10(4).

Kim, G.H., Pesaran, A., and Spotnitz, R. (2007). A three-dimensional thermal abuse model for lithium-ion cells. *Journal of power sources*, 170(2), 476–489.

Kizilel, R., Sabbah, R., Selman, J.R., and Al-Hallaj, S. (2009). An alternative cooling system to enhance the safety of li-ion battery packs. *Journal of Power Sources*, 194(2), 1105–1112.

Møller, K.T., Sheppard, D., Ravnsbæk, D.B., Buckley, C.E., Akiba, E., Li, H.W., and Jensen, T.R. (2017). Complex metal hydrides for hydrogen, thermal and electrochemical energy storage. *Energies*, 10(10), 1645.

Pesaran, A. (2013). Tools for designing thermal management of batteries in electric drive vehicles. Technical report, National Renewable Energy Laboratory. Accessed: 2024-12-06.

Safavi, V., Bazmohammadi, N., Vasquez, J.C., and Guerrero, J.M. (2024). Battery state-of-health estimation: A step towards battery digital twins. *Electronics*, 13(3), 587.

Saw, L.H., Ye, Y., and Tay, A.A. (2016). Integration issues of lithium-ion battery into electric vehicles battery pack. *Journal of Cleaner Production*, 113, 1032–1045.

Yunus, A.C. (2010). *Fluid Mechanics: Fundamentals And Applications (Si Units)*. Tata McGraw Hill Education Private Limited.